8

Pipes, Horns and Cavities

The wave propagation phenomena in fluids that we have examined in previous chapters have referred to waves in infinite or semi-infinite spaces generated by the vibrational motion of some small object or surface in that space. We now turn to the very different problem of studying the sound field inside the tube of a wind instrument. Ultimately, we shall join together the two discussions by considering the sound radiated from the open end or finger holes of the instrument, but for the moment our concern is with the internal field. We begin with the very simplest cases and then add complications until we have a reasonably complete representation of an actual instrument.

Pipes, cavities, and apertures are, however, also important in instruments other than those of the wind family, and we will later be concerned with sound fields inside both stringed and percussion instruments. We therefore take the opportunity to introduce the general methods of electric network analogs, which are very powerful yet very simple, for the analysis of such systems.

8.1 Infinite Cylindrical Pipes

The simplest possible system of enclosure is an infinite cylindrical pipe or tube with its axis parallel to the direction of propagation of a plane wave in the medium (Morse and Ingard, 1968). If the walls of the pipe are rigid, perfectly smooth, and thermally insulating, then the presence of the tube wall has no effect on wave propagation. A pressure wave propagating in the x direction has the form

$$p(x,t) = p\exp[j(-kx+\omega t)], \tag{8.1}$$

and the resultant acoustic volume flow is, as we saw in Chapter 6,

$$U(x,t) = \left(\frac{Sp}{\rho c}\right)\exp[j(-kx+\omega t)], \tag{8.2}$$

where ω is the angular frequency, k is the angular wave number $k = 2\pi/\lambda = \omega/c$, and S is the cross-sectional area of the pipe. As usual, ρ is the density of and c the velocity of sound in air. The acoustic impedance of the pipe at any point x is defined to be

$$Z_0(x) = \frac{p(x,t)}{U(x,t)} = \frac{\rho c}{S}. \tag{8.3}$$

To treat this problem in more detail, we must solve the wave equation directly in cylindrical polar coordinates (r, ϕ, x). If a is the radius of the pipe and its surface is again taken to be perfectly rigid, then the boundary condition is

$$\frac{\partial p}{\partial r} = 0 \quad \text{at} \quad r = a, \tag{8.4}$$

which implies that there is no net force and therefore no flow normal to the wall. The wave equation in cylindrical coordinates is

$$\frac{1}{r}\frac{\partial}{\partial r}\left(r\frac{\partial p}{\partial r}\right) + \frac{1}{r^2}\frac{\partial^2 p}{\partial \phi^2} + \frac{\partial^2 p}{\partial x^2} = \frac{1}{c^2}\frac{\partial^2 p}{\partial t^2}, \tag{8.5}$$

and this has solutions of the form

$$p_{mn}(r,\phi,x) = p^{\cos}_{\sin}(m\phi)J_m\left(\frac{\pi q_{mn} r}{a}\right)\exp[j(-k_{mn}x+\omega t)], \tag{8.6}$$

where J_m is a Bessel function and q_{mn} is defined by the boundary condition [Eq. (8.4)], so that the derivative $J'_m(\pi q_{mn})$ is zero. The (m, n) mode thus has an (r, ϕ) pattern for the acoustic pressure p with n nodal circles and m nodal diameters, both m and n running through the integers from zero. In the full three-dimensional picture, these become nodal cylinders parallel to the axis and nodal planes through the axis, respectively.

In Fig. 8.1, the pressure and flow velocity patterns for the lowest three modes of the pipe, omitting the simple plane-wave mode, are shown. The pressure patterns have nodal lines as already observed, and there are similar nodal diameters in the transverse flow patterns. Nodal circles for pressure occur for modes of the type $(0, n)$, which have n such nodal circles within the boundary. A general mode (m, n) has both nodal lines and circles in the pressure.

The propagation wave vector k_{mn} for mode (m, n) is obtained by substituting Eq. (8.6) into Eq. (8.5), whence

$$k_{mn}^2 = \left(\frac{\omega}{c}\right)^2 - \left(\frac{\pi q_{mn}}{a}\right)^2. \tag{8.7}$$

Thus, while the plane-wave mode with $m = n = 0$ will always propagate with $k = k_{00} = \omega/c$, this is not necessarily true for higher modes. In order for a higher mode (m, n) to propagate, the frequency must exceed the

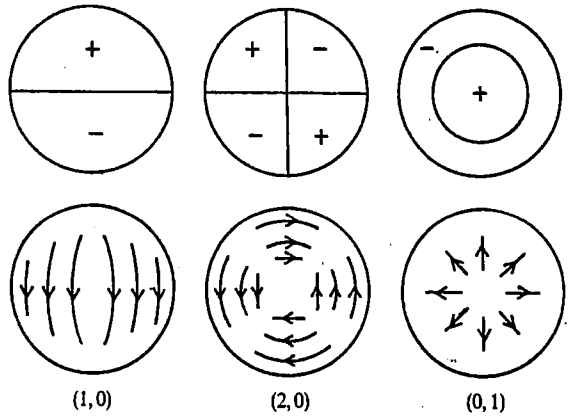

FIGURE 8.1. Pressure and transverse flow patterns for the lowest three transverse modes of a cylindrical pipe. The plane-wave mode is not shown.

critical value

$$\omega_c = \frac{\pi q_{mn} c}{a}. \tag{8.8}$$

For frequencies less than ω_c, k_{mn} is imaginary and Eq. (8.6) shows that the mode is attenuated exponentially with distance. The attenuation is quite rapid for modes well below cutoff, and the amplitude falls by a factor e, or about 10 dB, within a distance less than the pipe radius.

The first higher mode to propagate is the antisymmetric (1, 0) mode, which has a single nodal plane, above a cutoff frequency $\omega_c = 1.84c/a$. Next is the (2, 0) mode, with two nodal planes, for $\omega > 3.05c/a$, and then the lowest nonplanar axial mode (0, 1), for $\omega > 3.80c/a$. Propagating higher modes are thus possible only when the pipe is greater in diameter than about two-thirds of the free-space acoustic wavelength. The nonpropagating higher modes are necessary to explain certain features of the acoustic flow near wall irregularities, such as finger holes or mouthpieces. Indeed, it is possible to match any disturbance distributed over an opening or a vibrating surface in a duct with an appropriate linear combination of duct modes. The plane-wave component of this combination will always propagate along the duct away from the disturbance, but this will not be true for modes with q_{mn} values that are too large. The propagating wave will thus be a low-pass filtered version of the disturbance, while the nonpropagating modes will simply modify the flow in the near neighborhood of the source.

It is helpful to sketch the three-dimensional acoustic flow streamlines associated with a few of these modes for both propagating and nonpropagating cases. This can be done from the form of the pressure pattern given

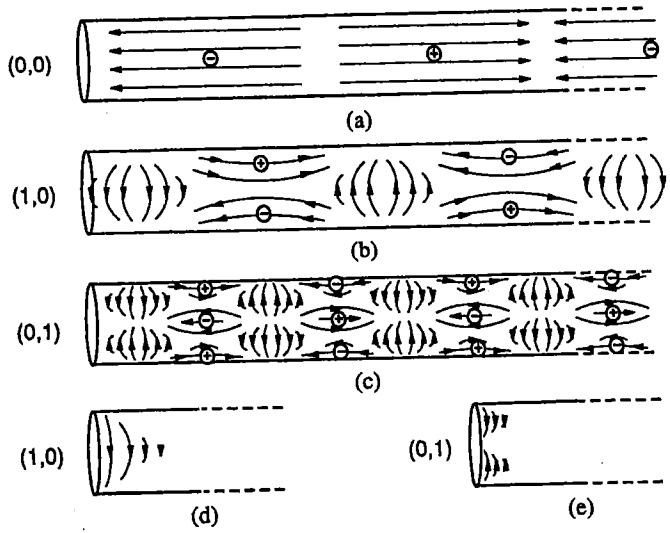

FIGURE 8.2. Acoustic flow patterns and pressure maxima and minima for higher modes in a cylindrical duct. (a)–(c) are modes propagating to the right at a frequency a little above cut-off; (d) and (e) are evanescent modes below cutoff.

by Eq. (8.6) together with the relation

$$u = \frac{j}{\rho\omega}\nabla \mathrm{p} \tag{8.9}$$

for the flow velocity u in a mode excited at frequency ω. Figure 8.2 shows this for the (1, 0) and (0, 1) modes. In the case of the propagating modes, the flow pattern itself moves down the pipe with the characteristic phase velocity of the mode—nearly the normal sound velocity c, except very close to cutoff when the phase velocity is higher than c.

It is not important to go into detail about the impedance behavior of these higher modes, since this depends greatly upon the geometry with which they are driven, the net acoustic flow along the pipe axis being zero except for the plane (0, 0) mode. The impedance is always a real function multiplied by ω/k_{mn}, so it is real for ω above cutoff, becomes infinite at cutoff, and is imaginary below cutoff.

8.2 Wall Losses

So far in our discussion, we have assumed a rigid wall without introducing any other disturbance. In a practical case this can never be achieved, though in musical instruments the walls are at least rigid enough that their

mechanical vibrations can be neglected—we return to the subtleties of this statement later. More important, however, are viscous and thermal effects from which no real walls or real fluids are immune.

Detailed consideration of these effects is complicated (Benade, 1968), but the basic phenomena and final results are easily discussed. The walls contribute a viscous drag to the otherwise masslike impedance associated with acceleration of the air in the pipe. The relative magnitude of the drag depends upon the thickness of the viscous boundary layer, itself proportional to the square root of the viscosity η divided by the angular frequency ω, in relation to the pipe radius a. A convenient parameter to use is the ratio of pipe radius to the boundary layer thickness:

$$r_v = \left(\frac{\omega\rho}{\eta}\right)^{1/2} a. \tag{8.10}$$

Similarly, thermal exchange between the air and the walls adds a lossy resistance to the otherwise compliant compressibility of the air, and the relative magnitude of this loss depends on the ratio of the pipe radius a to the thermal boundary layer thickness, as expressed by the parameter

$$r_t = \left(\frac{\omega\rho C_p}{\kappa}\right)^{1/2} a, \tag{8.11}$$

where C_p is the specific heat of air at constant pressure and κ is its thermal conductivity. The ratio $(r_t/r_v)^2 = C_p\eta/\kappa$ is the Prandtl number. Near 300 K (27°C), we can insert numerical values to give (Benade, 1968)

$$r_v \approx 632.8af^{1/2}(1 - 0.0029\,\Delta T), \tag{8.12}$$

and

$$r_t \approx 532.8af^{1/2}(1 - 0.0031\,\Delta T), \tag{8.13}$$

where a is the tube radius in meters, f is the frequency in hertz, and ΔT is the temperature deviation from 300 K.

It is clear that the effect of these loss terms will be to change the characteristic impedance Z_0 of the pipe from its ideal real value $\rho c/S$ to a complex quantity. This, in turn, will make the wave number k complex and lead to attenuation of the propagating wave as it passes along the pipe.

The real and imaginary parts of the characteristic impedance Z_0, as fractions of its ideal value $\rho c/S$, are shown in Figs. 8.3 and 8.4, both as functions of r_v. The correction to Z_0 begins to be appreciable for $r_v < 10$, while for $r_v < 1$ the real and imaginary parts of Z_0 are nearly equal and vary as r_v^{-1}.

It is convenient to rewrite the wave vector k as the complex number $\omega/v - j\alpha$, where α is now the attenuation coefficient per unit length of path and v is the phase velocity. We can then most usefully plot the phase velocity v, measured in units of the free-air sound velocity c, and the attenuation coefficient α, divided by f, both as functions of r_v. This is done in Figs. 8.5

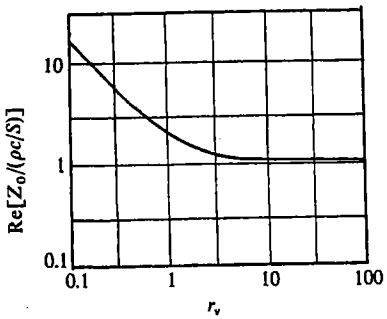

FIGURE 8.3. Real part of the characteristic impedance Z_0, in units of $\rho c/S$, as a function of the parameter r_v (after Benade, 1968).

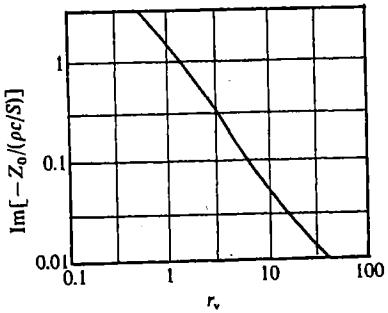

FIGURE 8.4. Imaginary part of the characteristic impedance Z_0, in units of $\rho c/S$, as a function of the parameter r_v (after Benade, 1968).

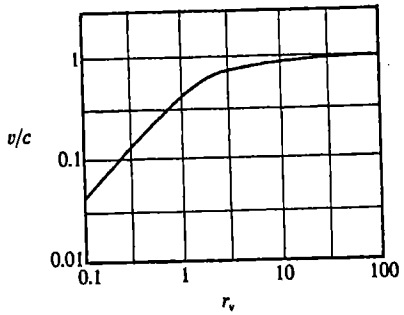

FIGURE 8.5. The phase velocity v, relative to the free-air sound velocity c, as a function of the parameter r_v (after Benade, 1968).

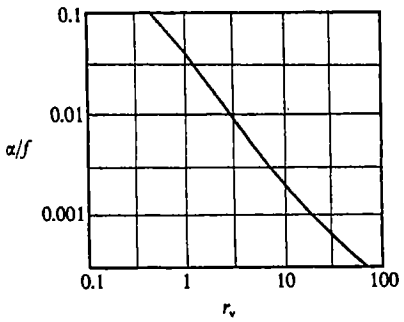

FIGURE 8.6. The attenuation coefficient α in (meters)$^{-1}$ at frequency f, plotted as α/f, as a function of the parameter r_v (after Benade, 1968).

and 8.6. The phase velocity v is significantly less than c for pipes so narrow that $r_v < 10$, while the attenuation coefficient exceeds λ^{-1} if $r_v < 6$. Since the phase velocity and attenuation coefficient for relatively wide tubes are both of fundamental significance for the physics of musical instruments, it is useful to restate Benade's (1968) versions of Rayleigh's (1894) approximate formulas, which are good for $r_v > 10$ and useful down to about $r_v = 3$. They are

$$v \approx c\left[1 - \frac{1}{r_v\sqrt{2}} - \frac{(\gamma-1)}{r_t\sqrt{2}}\right] \approx c\left[1 - \frac{1.65\times10^{-3}}{af^{1/2}}\right], \tag{8.14}$$

and

$$\alpha \approx \frac{\omega}{c}\left[\frac{1}{r_v\sqrt{2}} + \frac{(\gamma-1)}{r_t\sqrt{2}}\right] \approx \frac{3\times10^{-5}f^{1/2}}{a}, \tag{8.15}$$

where α is given in (meters)$^{-1}$ if a is in meters. Here, γ is the ratio of specific heats C_p/C_v, which for air is approximately 1.40.

In most of the more practical discussions that follow, we will find it adequate simply to use a complex form for k, with real and imaginary parts derived from Eqs. (8.14) and (8.15). The fact that Z_0 has a small imaginary part is not generally significant for the main pipes of musical instruments. For a few discussions, such as those related to the smaller tubes of finger holes, the more general results shown in the figures may be necessary.

8.3 Finite Cylindrical Pipes

All of the pipes with which we deal in musical instruments are obviously of finite length, so we must allow for the reflection of a wave from the

remote end, whether it is open or closed. Because we are concerned with pipes as closely coupled driven systems, rather than as passive resonators, we shall proceed by calculating the input impedance for a finite length of pipe terminated by a finite load impedance Z_L, rather than examining doubly open or closed pipes in isolation. The terminating impedance Z_L will generally represent an open or a closed end, but it is not restricted to these cases. The development here is essentially the same as that set out in Chapter 2 for a string stretched between nonrigid bridges but, since the results are central to our discussion of pipes and horns, we start again from the beginning.

Suppose the pipe extends from $x = 0$ to $x = L$, and that it is terminated at $x = L$ by the impedance Z_L. The pressure in the pipe is a superposition of two waves, moving to the right and left, respectively, with amplitudes A and B, taken as complex quantities so that they can include a phase factor. Thus, at the point x,

$$p(x,t) = [Ae^{-jkx} + Be^{jkx}]e^{j\omega t}. \tag{8.16}$$

The acoustic particle velocity is similarly a superposition of the particle velocities associated with these two waves and, multiplying by pipe cross section S, the acoustic flow becomes, from Eq. (8.3),

$$U(x,t) = \left(\frac{S}{\rho c}\right)[Ae^{-jkx} - Be^{jkx}]e^{j\omega t}. \tag{8.17}$$

At the remote end $x = L$, pressure and flow are related as required by the terminating impedance Z_L, so that

$$\frac{p(L,t)}{U(L,t)} = Z_L, \tag{8.18}$$

and this equation is enough to determine the complex ratio B/A. If we write for the characteristic impedance of the pipe

$$Z_0 = \rho c/S \tag{8.19}$$

as in Eq. (8.3), then

$$\frac{B}{A} = e^{-2jkL}\left[\frac{(Z_L - Z_0)}{(Z_L + Z_0)}\right], \tag{8.20}$$

and the power reflected from Z_L has a ratio to incident power of

$$R = \left|\frac{B}{A}\right|^2 = \left|\frac{Z_L - Z_0}{Z_L + Z_0}\right|^2. \tag{8.21}$$

Clearly, there is no reflection if $Z_L = Z_0$ and complete reflection if $Z_L = 0$ or ∞. Since Z_0 is real for a lossless tube, there is also perfect reflection if Z_L is purely imaginary; however, if Z_L has a real part that is nonzero, then there will always be some reflection loss.

The quantity in which we are interested now is the input impedance Z_{IN} at the point $x = 0$. From Eqs. (8.16)–(8.19), this is

$$Z_{IN} = Z_0 \left[\frac{A+B}{A-B} \right], \tag{8.22}$$

or from Eq. (8.20),

$$Z_{IN} = Z_0 \left[\frac{Z_L \cos kL + jZ_0 \sin kL}{jZ_L \sin kL + Z_0 \cos kL} \right]. \tag{8.23}$$

Two important idealized cases are readily derived. The first corresponds to a pipe rigidly stopped at $x = L$ so that $Z_L = \infty$. For such a pipe,

$$Z_{IN}^{\text{stopped}} = -jZ_0 \cot kL. \tag{8.24}$$

For the converse case of an ideally open pipe with $Z_L = 0$, which is not physically realizable exactly, as we see below,

$$Z_{IN}^{\text{open}} = jZ_0 \tan kL. \tag{8.25}$$

The familiar resonance frequencies for open and stopped pipes arise from applying the idealized condition that the input end at $x = 0$ is also open, so that resonances occur if $Z_{IN} = 0$. For a stopped pipe, this requires that $\cot kL = 0$, giving

$$\omega^{\text{stopped}} = \frac{(2n-1)\pi c}{2L}, \tag{8.26}$$

corresponding to an odd number of quarter wavelengths in the pipe length, while for an ideally open pipe, $\tan kL = 0$, giving

$$\omega^{\text{open}} = \frac{n\pi c}{L}, \tag{8.27}$$

corresponding to an even number of quarter wavelengths, or any number of half wavelengths, in the pipe length.

While Eq. (8.24) applies quite correctly to a physically stopped pipe, the treatment of a physically open pipe is more difficult since, while $Z_L \ll Z_0$, it is not a sufficient approximation to set it to zero. It is relatively straightforward to calculate the radiation load Z_L on a pipe that terminates in a plane flange of size much larger than a wavelength (and therefore effectively infinite). The formal treatment of Rayleigh (1894) (Morse, 1948, Olson, 1957) makes the assumption that the wavefront exactly at the open end of the pipe is quite planar, normally a very good approximation, and gives the result

$$Z^{\text{flanged}} = R + jX, \tag{8.28}$$

where, as discussed for Eqs. (7.32)–(7.34),

$$R = Z_0 \left[\frac{(ka)^2}{2} - \frac{(ka)^4}{2^2 \cdot 3} + \frac{(ka)^6}{2^2 \cdot 3^2 \cdot 4} - \cdots \right], \tag{8.29}$$

$$X = \frac{Z_0}{\pi k^2 a^2} \left[\frac{(2ka)^3}{3} - \frac{(2ka)^5}{3^2 \cdot 5} + \frac{(2ka)^7}{3^2 \cdot 5^2 \cdot 7} - \cdots \right], \tag{8.30}$$

and a is the radius of the pipe.

The behavior of R and X as functions of frequency, or more usefully as functions of the dimensionless quantity ka, is shown in Fig. 8.7. If $ka \ll 1$, then $|Z^{\text{flanged}}| \ll Z_0$ and most of the wave energy is reflected from the open end. If $ka > 2$, however, then $Z^{\text{flanged}} \approx Z_0$ and most of the wave energy is transmitted out of the end of the pipe into the surrounding air.

In musical instruments, the fundamental, at least, has $ka \ll 1$, though this is not necessarily true for all the prominent partials in the sound. It is therefore useful to examine the behavior of the pipe in this low-frequency limit. From Eqs. (8.29) and (8.30), $X \gg R$ if $ka \ll 1$, so that

$$Z^{\text{flanged}} \approx jZ_0 k \left(\frac{8a}{3\pi} \right). \tag{8.31}$$

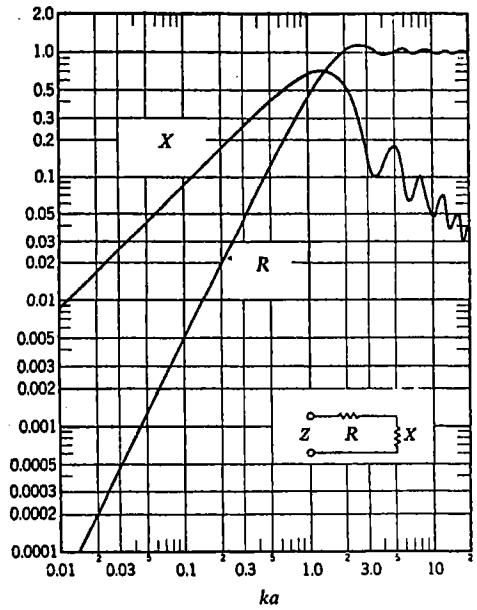

FIGURE 8.7. The acoustic resistance R and the acoustic reactance X, both in units of $\rho c/\pi a^2$, for a circular piston (or open pipe) of radius a set in an infinite plane baffle, as functions of the frequency parameter ka (after Beranek, 1954).

By comparison with Eq. (8.25), since $ka \ll 1$, this is just the impedance of an ideally open short pipe of length

$$\Delta^{\text{flanged}} = \frac{8a}{3\pi} \approx 0.85a. \tag{8.32}$$

It is thus a good approximation in this frequency range to replace the real flanged pipe by an ideally open pipe of length $L + \Delta^{\text{flanged}}$, and to neglect the radiation loss. From Fig. 8.7, it is clear that the end correction Δ^{flanged}, which is proportional to X/ka, decreases slightly as $ka \to 1$ and continues to decrease more rapidly as ka increases past this value.

A real pipe, of course, is not generally flanged, and we need to know the behavior of Z_L in this case. The calculation (Levine and Schwinger, 1948) is very difficult, but the result, as shown in Fig. 8.8, is very similar to that for a flanged pipe. The main difference is that, for $ka \ll 1$, R is reduced by about a factor 0.5 and X by a factor 0.7 because the wave outside the pipe has freedom to expand into a solid angle of nearly 4π rather than just 2π. The calculated end correction at low frequencies is now

$$\Delta^{\text{open}} \approx 0.61a. \tag{8.33}$$

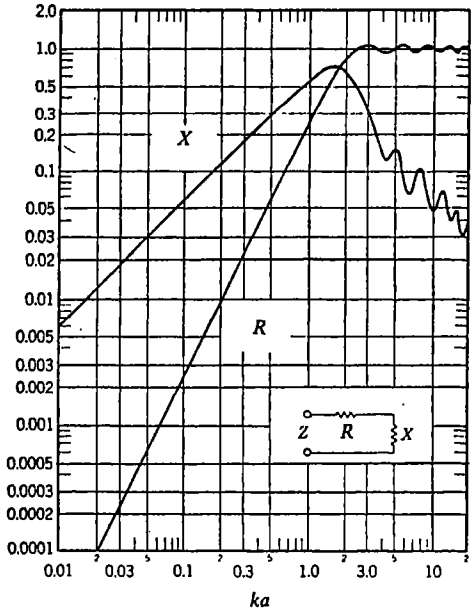

FIGURE 8.8. The acoustic resistance R and the acoustic reactance X, both in units of $\rho c/\pi a^2$ for the open end of a circular cylindrical pipe of radius a, as functions of the frequency parameter ka (after Beranek, 1954).

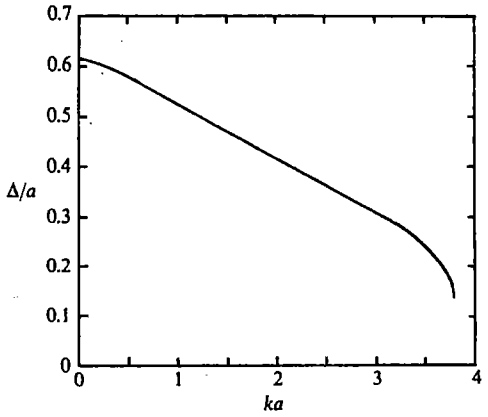

FIGURE 8.9. The calculated end correction Δ for a cylindrical pipe of radius a, plotted as Δ/a, as a function of the frequency parameter ka, (after Levine and Schwinger, 1948).

The calculated variation of this end correction with the frequency parameter ka is shown in Fig. 8.9.

8.4 Radiation from a Pipe

One of our later interests, of course, will be to calculate the sound radiation from musical wind instruments and, as part of this task, it is helpful to know the transformation function between the spectrum of sound energy within the pipe and the total radiated sound energy. This transformation is simply proportional to the behavior of R as a function of frequency, so that, to a good approximation, it rises as (frequency)^2, that is, 6 dB per octave, below the reflection cutoff frequency, defined so that $ka = 2$. Above this frequency, the transformation is independent of frequency. This remark refers, of course, to the total radiated power and neglects directional effects that tend to concentrate the higher frequencies at angles close to the pipe axis.

It is useful to summarize these directional effects here, since they are derived in the course of calculation of the radiation impedance Z_L. The flanged case is simplest (Rayleigh, 1894; Morse, 1948) and gives a radiated intensity at angle θ to the pipe axis proportional to

$$\left[\frac{2J_1(ka\sin\theta)}{ka\sin\theta}\right]^2. \tag{8.34}$$

The result for an unflanged pipe (Levine and Schwinger, 1948) is qualitatively similar except, of course, that θ can extend from 0 to 180° instead of just to 90°. The angular intensity distribution for this case is shown in Fig. 8.10 for several values of ka, the results being normalized to the power radiated along the axis (Beranek, 1954). The directional index (DI) is the intensity level on the axis compared to the intensity level produced by an isotropic source with the same total radiated power. The trend toward a narrower primary beam angle along the pipe axis continues for values of ka larger than those shown.

8.5 Impedance Curves

Finally, in this discussion, we should consider the behavior of pipes with physically realistic wall losses. Provided the pipe is not unreasonably narrow, say $r_v > 10$, then Figs. 8.3 and 8.4 show that we can neglect the small change in the characteristic impedance Z_0 and simply allow the possibility that k is complex for propagation in the pipe. This new k is written $(\omega/v - j\alpha)$ with v given by Eq. (8.14) and α given by Eq. (8.15). This can be simply inserted into Eq. (8.23), along with the appropriate expression for Z_L, to deduce the behavior of the input impedance of a real pipe. The result for an ideally open pipe ($Z_L = 0$) of length L is

$$Z_{IN} = Z_0 \left[\frac{\tanh \alpha L + j \tan(\omega L/v)}{1 + j \tanh \alpha L \tan(\omega L/v)} \right]. \tag{8.35}$$

This expression has maxima and minima at the maxima and minima, respectively, of $\tan(\omega L/v)$. The value of Z_{IN} at the maxima is $Z_0 \coth \alpha L$, and at the minima it is $Z_0 \tanh \alpha L$. By Eq. (8.15), α increases with frequency as $\omega^{1/2}$, so these extrema decrease in prominence at higher frequencies, and Z_{IN} converges toward Z_0. For a pipe stopped at the far end, the factor in square brackets in Eq. (8.35) should simply be inverted.

For narrow pipes the lower resonances are dominated by this wall-loss mechanism, but for wider open pipes radiation losses from the end become more important, particularly at high frequencies. To illustrate some features of the behavior, we show in Fig. 8.11 calculated impedance curves for two pipes each 1 m long and with diameters, respectively, 2 cm and 10 cm. The low-frequency resonances are sharper for the wide pipe than for the narrow pipe because of the reduced relative effect of wall damping, but the high-frequency resonances of the wide pipe are washed out by the effects of radiation damping. We can see that all the impedance maxima and minima have frequencies that are nearly harmonically related, that is, as the ratio of two small integers. In fact, because the end correction decreases with increasing frequency, the frequencies of these extrema are all slightly stretched, and this effect is more pronounced for the wide than for the narrow pipe.

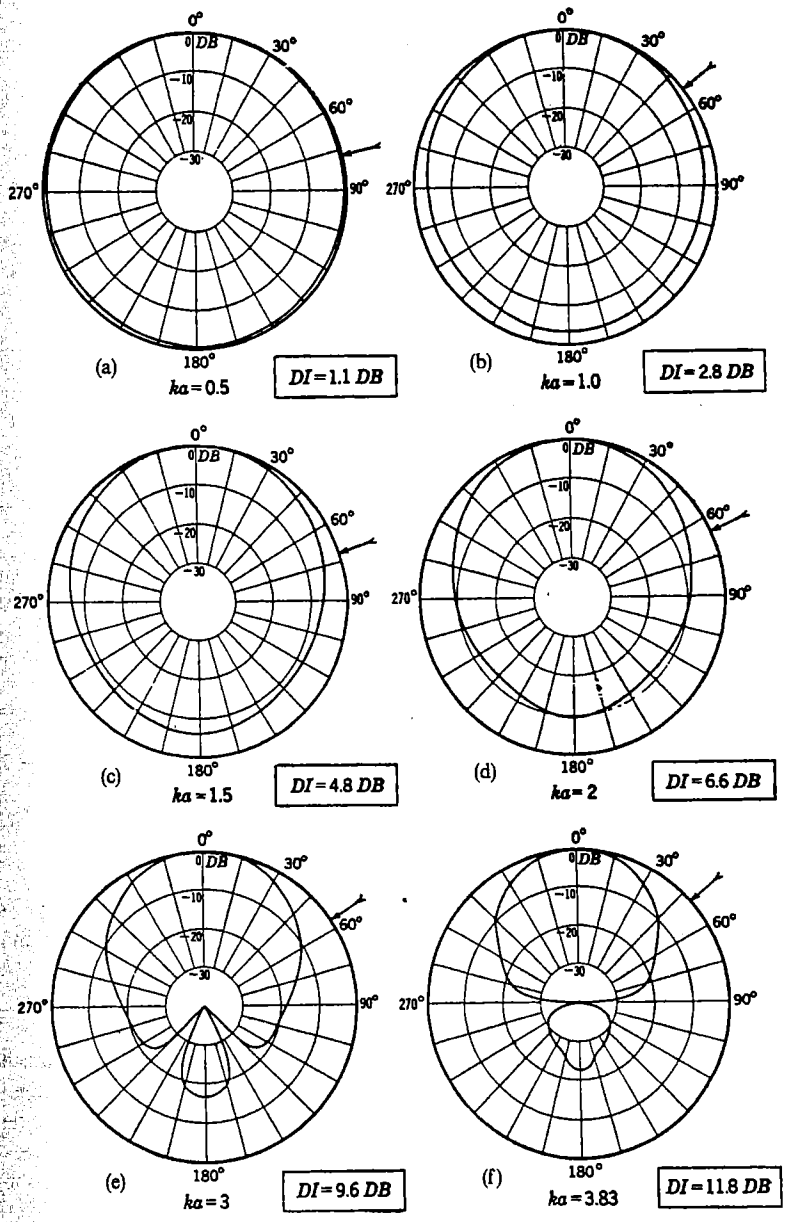

FIGURE 8.10. The directional patterns calculated by Levine and Schwinger for radiation from an unbaffled circular pipe of radius a. The radial scale is in each case 40 dB and the directional index has the calculated value shown (after Beranek, 1954).

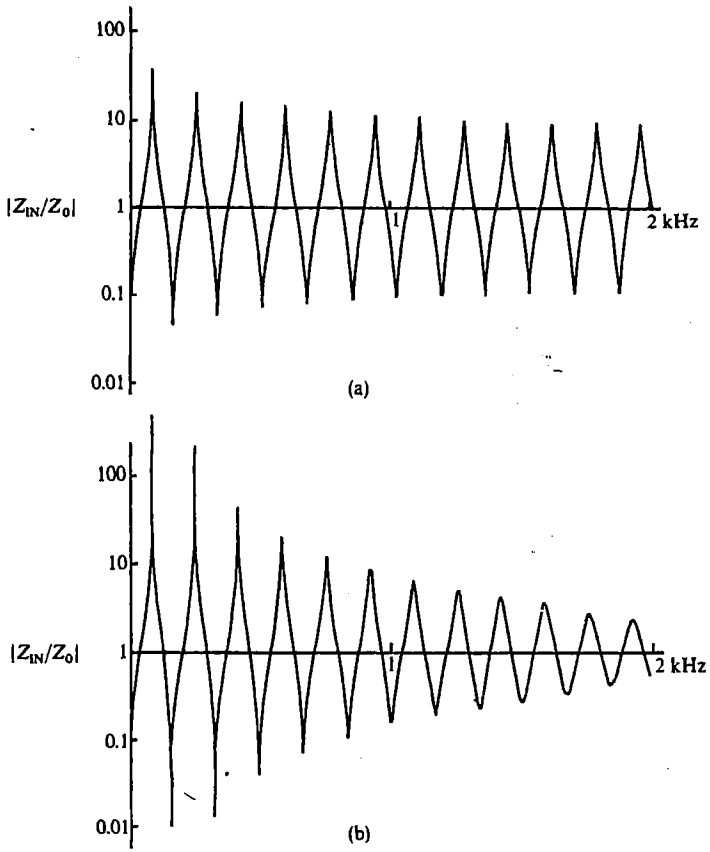

FIGURE 8.11. Magnitude of the acoustic input impedance Z_{IN}, in terms of the characteristic impedance Z_0, for open cylindrical pipes of length 1 m and diameters of (a) 2 cm and (b) 10 cm.

It is worthwhile to note incidentally that, because these input impedance curves have been plotted on a logarithmic scale, the corresponding admittance curves can be obtained simply by turning the impedance curve upside down. We will see later that sometimes we will be required to think of admittance maxima and sometimes of impedance maxima, depending upon the way in which the pipe is used.

When we come to consider musical instruments in detail, we will find that several of them rely upon cylindrical pipes as their sound generators. The most obvious of these is the pipe organ, in which most of the pipes are cylindrical (a few are conical). Tone quality of air-jet-driven pipes is varied by the use of closed and open tubes, by differences in relative diameters, and by differences in the sort of termination at the open end—some are simple open ends, some have slots, some have bells, and some have narrow chimneys. These variations can all be treated on the basis of the above discussion supplemented by a separate consideration of the form of Z_L produced by the termination.

8.6 Horns

Following this introductory discussion of cylindrical pipes, we are now ready to begin a treatment of sound propagation in horns, a horn being defined quite generally as a closed-sided conduit, the length of which is usually large compared with its lateral dimensions. In fact, we shall only treat explicitly horns that are straight and have circular cross section, but much of the discussion is really more general than this. A mathematically detailed discussion of the topic, with copious references, has been given by Campos (1984).

Formulation of the wave propagation problem in an infinitely long horn simply requires solution of the wave equation

$$\nabla^2 p = \frac{1}{c^2}\frac{\partial^2 p}{\partial t^2}, \tag{8.36}$$

subject to the condition that $\mathbf{n}\cdot\nabla p = 0$ on the boundaries, $\mathbf{n}$ being a unit vector normal to the boundary at the point considered. More simply, we suppose the wave to have a frequency ω so that Eq. (8.36) reduces to the Helmholtz equation

$$\nabla^2 p + k^2 p = 0, \tag{8.37}$$

where $k = \omega/c$. Solution of this equation is simple provided that we can choose a coordinate system in which one coordinate surface coincides with the walls of the horn and in which Eq. (8.37) is separable. Unfortunately, the Helmholtz equation is separable only in coordinates that are confocal quadric surfaces or their degenerate forms (Morse and Feshbach, 1953). There are 11 varieties of these coordinate systems, but only a few of them are reasonable candidates for horns. These are rectangular coordinates (a pipe of rectangular cross section), circular cylinder coordinates, elliptic cylinder coordinates, spherical coordinates (a conical horn), parabolic coordinates, and oblate spheroidal coordinates, as shown in Fig. 8.12. Of these, we have already dealt with the circular cylinder case, and the rectangular and elliptic cylinder versions differ from it only in cross-sectional geometry and hence in their higher modes. The parabolic horn is not musically practical since it cannot be made to join smoothly onto a mouthpiece, so we are left with the conical horn and the horn derived from oblate spheroidal coordinates, which will prove to be of only passing interest.

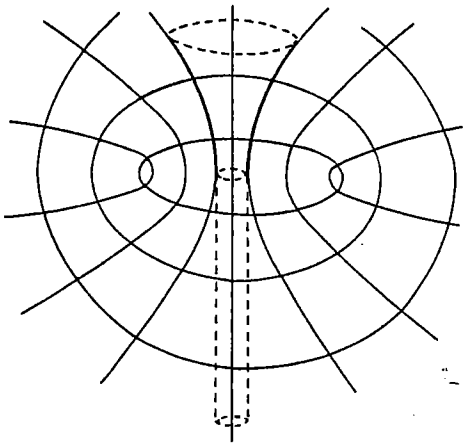

FIGURE 8.12. The oblate spheroidal coordinate system in which the wave equation is separable. If the hyperboloid of revolution (shown in heavy outline) is taken as the horn, then the oblate spheroidal surfaces orthogonal to this and lying within it are the wave fronts. Note that such a hyperboloid horn can be smoothly joined to a cylindrical pipe of appropriate diameter, as shown.

We deal with the oblate spheroidal case first, because it illustrates some of the difficulties we will have to face later. The hornlike family of surfaces consists of hyperboloids of revolution of one sheet, as shown in Fig. 8.12. At large distances, these approach conical shapes, but near the origin they become almost cylindrical. Indeed, one could join a simple cylinder parallel to the axis in the lower half plane to a hyperboloid horn in the upper half plane without any discontinuity in slope of the walls. The important thing to notice, however, is the shape of the wavefronts as shown by the orthogonal set of coordinate surfaces. These are clearly curved and indeed they are oblately spheroidal, being nearly plane near the origin and nearly spherical at large distances. Waves can propagate in this way as a single mode, like the plane waves in a cylinder. Such behavior is possible only for separable coordinate systems. For nonseparable systems that we may try to separate approximately, there will always be an admixture of higher modes. Horn systems resembling a cylinder joined to a narrow-angle hyperboloid horn as described above are in fact used in many brass instruments, though not because of any consideration of separability of the wave equation. Indeed, once the length of the horn is made finite, we produce an unresolvable inseparability near the open end so that there is no real practical design assistance derived from near separability inside the horn.

Rather than setting out the exact solution for a hyperboloid or a conical horn in detail, let us now go straight to the approximate solution for propagation in an infinite horn of rather general shape. We assume that we have

some good approximation to the shapes of the wavefronts—something more or less spherical and, since the wave fronts must be orthogonal to the horn walls, centered approximately at the apex of the cone that is locally tangent to the horn walls, as shown in Fig. 8.13. This description will be exact for a conical horn, but only an approximation for other shapes. If $S(x)$ is the area of this wavefront in the horn at position x, defined by its intersection with the axis, then, during an acoustic displacement ξ, the fractional change in the volume of air in the horn at position x is $(1/S)\partial(S\xi)/\partial x$. This contrasts with the simpler expression $\partial\xi/\partial x$ for a plane wave in unconfined space. Proceeding now as for the plane-wave case, we find a wave equation of the form

$$\frac{1}{S}\frac{\partial}{\partial x}\left(S\frac{\partial p}{\partial x}\right) = \frac{1}{c^2}\frac{\partial^2 p}{\partial t^2}, \tag{8.38}$$

which is known as the Webster equation (Webster, 1919; Eisner, 1967), although its origins date back to the time of Bernoulli. Actually, in Webster's case, the curvature of the wave fronts was neglected so that x was taken as the geometrical distance along the horn axis and S as the geometrical cross section at position x. This plane-wave approximation is good for horns that are not rapidly flaring, but breaks down for a horn with large flare. Various simple modifications to the Webster equation have been proposed (Weibel, 1955; Keefe et al., 1993), all of which improve its approximation by replacing the plane-wave surfaces by curved surfaces, chosen so as to meet the horn surface and the axis normally. All essentially ignore the transverse flow that is necessitated by the fact that an elementary volume element between successive wavefronts is thicker on the axis than at its edges, and simply assume constant pressure throughout the element.

Here, as well, we have assumed that p is constant across the wave front in the horn, which is equivalent to assuming separability. This is not a bad approximation for horns that do not flare too rapidly, but we must not expect too much of it in extreme cases. In this spirit, we now make the transformation

$$p = \psi S^{-1/2} \tag{8.39}$$

in the reasonable expectation that, with the even spreading of wave energy across the wavefront, ψ should be essentially constant in magnitude, independent of x. If we also assume that p varies with angular frequency ω and write S in terms of a local equivalent radius a so that

$$S = \pi a^2, \tag{8.40}$$

then Eq. (8.38) becomes

$$\frac{\partial^2\psi}{\partial x^2} + \left(k^2 - \frac{1}{a}\frac{\partial^2 a}{\partial x^2}\right)\psi = 0, \tag{8.41}$$

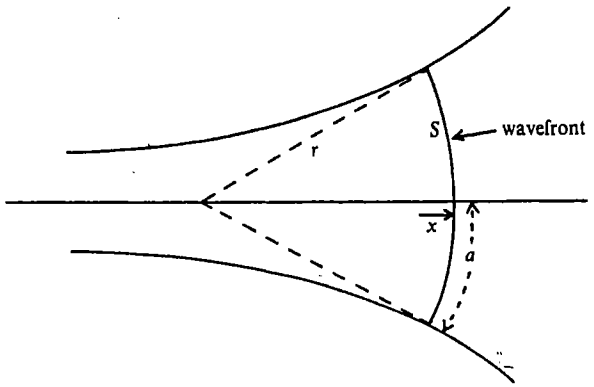

FIGURE 8.13. In a horn, the wavefront has approximately the form of a spherical cap of area S and effective radius r based upon the local tangent cone and cutting the axis at a point with coordinate x.

where $k = \omega/c$. This form of the equation, noted by Stevenson (1951) and later by Benade and Jansson (1974), serves as a good basis for discussion of the behavior of horns. In a formal sense, it is the exact analog of the Schrödinger equation in quantum mechanics, with the "horn function"

$$F \equiv \frac{1}{a}\frac{d^2a}{dx^2} = \frac{1}{2S}\frac{\partial^2 S}{\partial x^2} - \frac{1}{4S^2}\left(\frac{\partial S}{\partial x}\right)^2 \tag{8.42}$$

taking the place of the potential.

The important thing to notice about Eq. (8.41) is that the wave function ψ, and hence the original pressure wave p, is propagating or nonpropagating according as $k^2 \gtrless F$, which is just what we would expect for a quantum particle of normalized energy k^2 meeting a potential barrier. The frequency $\omega = kc$ for which we have equality is called the cutoff frequency at this part of the horn. A visual estimate of the magnitude of F at a given position x can be made, as illustrated in Fig. 8.14, by observing that a is essentially the transverse radius of curvature R_T of the horn at point x while $(d^2a/dx^2)^{-1}$ is close to the external longitudinal radius of curvature R_L, provided that the wall slope da/dx is small. Thus,

$$F \approx \frac{1}{R_L R_T}. \tag{8.43}$$

Of course, this is no longer a good approximation when the wall slope, or local cone angle, is large, and we must then use the expression

$$F = \frac{1}{a}\frac{d^2a}{dx^2}, \tag{8.44}$$

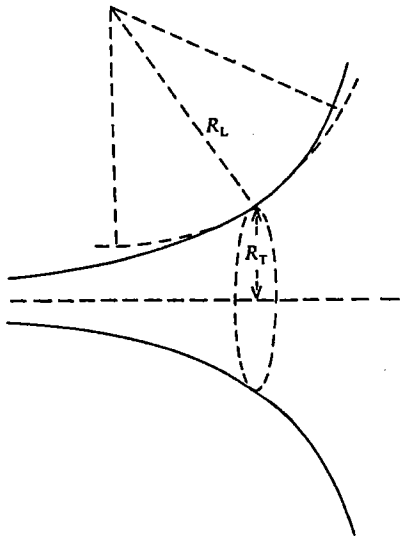

FIGURE 8.14. The geometry of a horn at any one place is characterized by the external longitudinal radius of curvature R_L and the internal transverse radius of curvature R_T.

with a interpreted as the equivalent internal radius measured along the wavefront as discussed previously.

Of particular theoretical simplicity is the class of horns called Salmon horns (Salmon, 1946a, b), for which the horn function F, and therefore the cutoff frequency ω_0, is constant along the whole length of the horn (Morse, 1948). Clearly, from Eq. (8.44), this implies

$$a = Ae^{mx} + Be^{-mx}, \tag{8.45}$$

where $F = m^2$ and m is called the flare constant. It is more convenient to rewrite Eq. (8.45) as

$$a = a_0[\cosh(mx) + T\sinh(mx)], \tag{8.46}$$

where T is an alternative parameter. The pressure wave in the horn then has the form

$$p = \left(\frac{p_0}{a}\right) e^{j\omega t} e^{-j\sqrt{k^2-m^2}x} \tag{8.47}$$

and is nonpropagating if $k < m$. These expressions should strictly all be interpreted in terms of curved wavefront coordinates, as in Fig. 8.13, but it is usual to neglect this refinement and simply use the plane-wave approximation.

The family of horns described by Eq. (8.46) has several important degenerate forms. If $T = 1$, then we have an exponential horn:

$$a = a_0 \exp(mx). \tag{8.48}$$

If $T = 0$, then we have a catenoidal horn:

$$a = a_0 \cosh(mx), \tag{8.49}$$

which has the nice feature of joining smoothly to a cylindrical pipe extending along the negative x axis to the origin, as was the case for the hyperboloidal horn. If $T = 1/mx_0$ and $m \to 0$, then we have a conical horn:

$$a = a_0 \left(1 + \frac{x}{x_0}\right), \tag{8.50}$$

with its vertex at $-x_0$ and a semiangle of $\tan^{-1}(a_0/x_0)$. Consideration of the value of the horn function given by Eq. (8.44) shows that $F = 0$ for this case, so that the conical horn has no cutoff.

Many of the applications of horns that are discussed in textbooks involve situations in which the diameter of the open end of the horn is so large that there is no appreciable reflection. The horn then acts as an efficient impedance transformer between a small diaphragm piston in the throat and a free spherical wave outside the mouth. Exponential and catenoidal horns have near-unity efficiency, as defined by Morse (1948), above their cutoff frequencies, while the efficiency of a conical horn never becomes zero but rises gradually with increasing frequency until it reaches unity. We shall not discuss these situations further—those interested should consult Morse (1948) or Olson (1957).

8.7 Finite Conical Horns

It is useful to quote results analogous to Eq. (8.23) for the throat impedance of a truncated conical or exponential horn terminated by a mouth impedance Z_L. Typically this might be the radiation impedance at an open mouth, for which we can use the expressions in Section 8.3, though these require some modification in careful work because of the curvature of the wavefronts (Fletcher and Thwaites, 1988). Another case of some interest is that in which the remote end of the horn is stopped rigidly so that $Z_L = \infty$.

For a conical horn with a throat of area S_1 located at position x_1, a mouth of area S_2 at position x_2, and length $L = x_2 - x_1$, we find (Olson, 1957)

$$Z_{IN} = \frac{\rho c}{S_1}\left\{\frac{jZ_L[\sin(kL-\theta_2)/\sin\theta_2] + (\rho c/S_2)\sin kL}{Z_L[\sin(kL+\theta_1-\theta_2)/\sin\theta_1\sin\theta_2] - (j\rho c/S_2)[\sin(kL+\theta_1)/\sin\theta_1]}\right\}, \tag{8.51}$$

where $\theta_1 = \tan^{-1} kx_1$ and $\theta_2 = \tan^{-1} kx_2$, both x_1 and x_2 being measured along the axis from the position of the conical apex. Similarly, for an exponential horn of the form of Eq. (8.48) and length L,

$$Z_{IN} = \frac{\rho c}{S_1}\left[\frac{Z_L\cos(bL+\theta) + j(\rho c/S_2)\sin bL}{jZ_L\sin bL + (\rho c/S_2)\cos(bL-\theta)}\right], \tag{8.52}$$

where $b^2 = k^2 - m^2$ and $\theta = \tan^{-1}(m/b)$. It is not simple to allow for wall effects in these expressions, since the imaginary part of k varies with position in the horn. For a horn with a wide mouth and not too narrow a throat, radiation effects may dominate so that k can be taken as real. This is, however, not a valid approximation in musical instruments, which use long horns of quite small diameter. We shall see that more complex calculations are necessary in such cases.

The expression [Eq. (8.51)] for the input impedance of a conical horn, measured at the end that is at a distance x_1 from the apex, deserves some further discussion. In the first place, we should note that it is applicable for the impedance at either the wide or the narrow end of a conical pipe. For a flaring cone, $x_2 > x_1$ and $L > 0$, while for a tapering cone, $x_2 < x_1$ and $L < 0$.

In the second place, we should examine several special cases of open and stopped cones, making the approximation that $Z_L = 0$ at an open end and $Z_L = \infty$ at a closed end. For a cone of length L with an ideally open end $Z_L = 0$, Eq. (8.51) gives, for either the large or the small end of a cone, the formal result

$$Z_{IN} = j\left(\frac{\rho c}{S_1}\right)\frac{\sin kL\sin\theta}{\sin(kL+\theta_1)}, \tag{8.53}$$

This does not imply that the input impedance is the same from both ends, since, as noted above, the sign of L and the magnitude of θ_1 are different in the two cases.

Zeros in Z_{IN} occur at frequencies for which $\sin kL = 0$, so that these frequencies are the same in each case and exactly the same as those for a cylindrical pipe with the same length L. To allow for the finite reactance associated with the radiation impedance Z_L, it is approximately correct, for a narrow cone, to simply add an appropriate end correction equal to 0.6 times the open end radius to the geometrical length L, as discussed in relation to Eq. (8.33).

The infinities in Z_{IN} occur, however, at frequencies that differ between the two cases and are not simply midway between those of the zeros, as was the case with a cylindrical pipe. Rather, the condition for an infinity in Z_{IN} is, from Eq. (8.53),

$$\sin(kL + \theta_1) = 0, \tag{8.54}$$

or equivalently,

$$kL = n\pi - \tan^{-1} kx_1. \tag{8.55}$$